Int. J. Multiphase Flow, Vol. 3, pp. 35–50. Pergamon/Elsevier, 1976. Printed in Great Britain.

EFFECT OF WALL FRICTION AND VORTEX GENERATION ON THE RADIAL DISTRIBUTION OF DIFFERENT PHASES

ZIA ROUHANI
Aktiebolaget Atomenergi Studsvik, Fack, Nykoping 61101, Sweden

(*Received* 9 *December* 1974)

Abstract—Arguments are presented to prove the existence of rolling vortices in single-phase and two-phase flow. In the liquid phase, they appear in a boundary layer near a wall while in the continuous vapor phase they occur near the interface with a liquid film. The intensity and size of these vortices depend on the local velocity gradients normal to the wall. The interaction between the rotational field associated with such vortices and bubbles in liquid flow or droplets in vapor flow is discussed. This interaction may be called the wall-vortex effect. It appears that several, apparently unrelated, phenomena observed in two-phase flow systems may be interpreted in terms of this mechanism. Among these are: (i) radial void peaking near the walls (ii) vapor velocities less than liquid velocity observed also in vertical upward flow (iii) reduced droplet diffusion near the liquid film and (iv) reduced vapor mixing between subchannels at low steam qualities. The cause of secondary flows in non-circular channels may also be explained in terms of rolling vortices near the walls. Finally, a comparison is made with the well known Magnus effect.

1. INTRODUCTION

Experimental studies of phase distribution in cocurrent flow of liquid–gas mixtures show a complex picture that has not yet received a proper explanation.

The complexity is not limited to the instantaneous pattern of phase distribution; it also applies to the time-averaged profiles of vapor or liquid fraction along any radius in a channel. However, the various distribution profiles are reproducible and, when carefully studied, demonstrate a systematic dependence on mass velocity, average vapor volume fraction (void) and channel geometry.

Staub & Zuber (1964) reported radial void distribution data obtained in a round tube of 10 mm I.D. These data indicated that the local void fraction peaked near the walls at low qualities and that this local peaking increased with increasing mass velocity. Further data of this kind were subsequently reported by Kroeger & Zuber (1966). Shires & Riley (1966) reported some data on radial void distribution in a round duct with air–water flow.

Malnes (1966) made systematic studies of radial void distribution both in air–water and in steam–water flow in round tubes. The air–water tests were performed with tube diameters of 26.3 mm and 46 mm. The liquid velocities varied from 0.2 to 4 m/s. The interesting result of these studies was a series of diagrams which indicated a definite occurrence of the peaking of air bubbles near the tube walls, at low values of average void, and the increase in this tendency with increasing liquid velocity. Figures 1 and 2 compare two cases with measured profiles taken from the data reported by Malnes (1966).

The diagrams show that the peak value of the local voids appears at a small distance from the wall and that the peaking is influenced by the average liquid velocity. Figure 3 (from the same source) indicates that repeated measurements at two different heights show no reduction in the void peaking near the walls.

Further data on radial void distribution are reported by Staub & Walmet (1969), Shiralkar (1970) and Dix (1971); all demonstrate a similar trend.

A review of the published data confirms the impression that there must be a mechanism which brings the center of bubble concentration to within a small distance from the walls independently of the mechanism of bubble generation in the flow.

This paper is devoted to the general phenomenon of vortex generation near solid walls and its plausible influence on phase distribution along a normal to a wall. The phenomenon of vortex

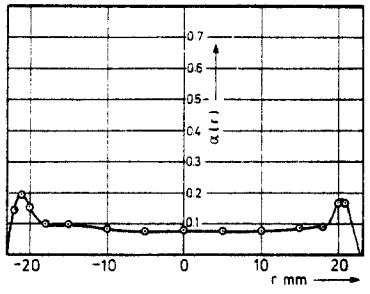

VOID PROFILE, 46mm, U_l = 0.6 m/s, α = 0.102, RUN 357

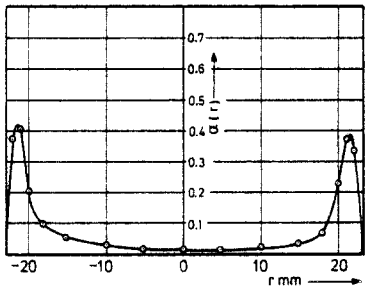

VOID PROFILE, 46mm, U_l = 1.5 m/s, α = 0.11, RUN 363

Figure 1. Comparison of two cases of radial void distribution in air–water flow, with roughly the same average void but different liquid velocities. Data reported by Malnes (1966) (Source KR-110).

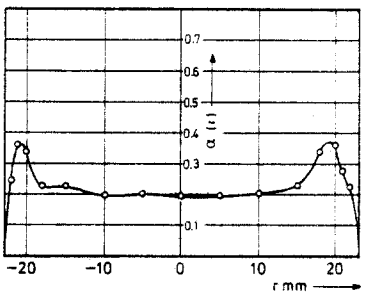

VOID PROFILE, 46mm, U_l = 0.6m/s, α = 0.227, RUN 358

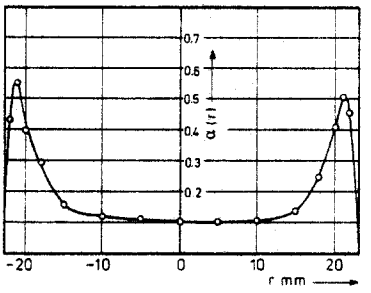

VOID PROFILE, 46mm, U_l = 1.5 m/s, α = 0.23, RUN 364

Figure 2. Comparison of two cases of radial void distribution in air–water flow, with roughly the same average void but different liquid velocities. Data reported by Malnes (1966) (Source KR-110).

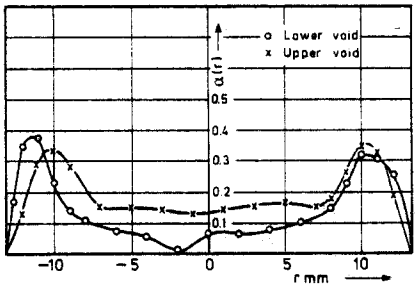

VOID PROFILES, 26.3 mm, U_l = 1.0 m/s, α = 0.201, RUN 340

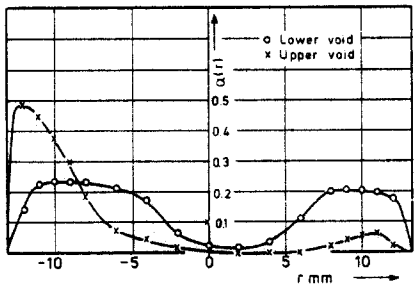

VOID PROFILES, 26.3 mm, U_l = 2.0 m/s, α = 0.159, RUN 355

Figure 3. A demonstration of the stability of the radial void peaking near the walls. Data reported by Malnes (1966).

generation is first discussed briefly for the case of single-phase flow and then extended to two-phase flow systems. The practical importance of these considerations relates to several aspects of two-phase flow, as will be described later. The effect of rolling vortices on the radial distribution of vapor and liquid is quite different from the well known Magnus effect, as is explained in appendix B.

2. THE STRUCTURE OF THE TURBULENT BOUNDARY LAYER

There are many treatises on the turbulent boundary layer, but very few deal with the actual structure of flow in that zone. In almost all published work the boundary layer has been treated on the basis of some mean and fluctuating velocity components in various directions. The literature contains elaborate mathematical treatments of the velocity distribution, based either on the phenomenological concept of mixing length theory, as given by Schlichting (1960) and Brodkey (1967), or on a purely statistical theory of fluctuations, as by Brodkey (1967). But none deals with the actual pattern of motion of the fluid particles within the turbulent layer.

Of particular interest to the present discussion is the visual observation of flow behaviour within the turbulent boundary layer. An interesting study of this kind is reported by Kline *et al.* (1967). In this work the authors present a considerable amount of material and argument, based on measurements and visual studies of various velocity components within the boundary layer, supporting the concept of the formation of rolling vortices near the walls. Kline *et al.* (1967) refer to a model suggested by Lighthill (1963) who considered the existence of a turning process within the boundary layer. The rolling vortices are called wall-layer streaks and Kline *et al.* derived a relationship between the frequency of breakup, average spacing of the streaks, and the shear velocity.

Although the general pattern of the turbulent boundary layer may be somewhat chaotic and shapeless, one may still expect that there is a dominance of rotational motion in a certain direction. This is dictated by the supply of linear momentum, contributed by the fluid particles which enter from the main flow, and the decelerating effect of viscosity in the viscous sublayer.

3. ROLLING VORTICES IN TWO-PHASE FLOW

In single-phase flow the thickness of the viscous sublayer and that of the so called buffer layer is affected both by the kinematic viscosity and the flow velocity. A mathematical relationship between these factors is given in the universal velocity distribution law, according to which the thickness of various layers decreases with decreasing kinematic viscosity and with increasing velocity. In terms of vortex generation on the walls this may be interpreted as a decrease in the average diameter of rolling vortices with either decreasing viscosity or increasing velocity. This interpretation fits the general observation that in turbulent flow, the friction factor decreases with increasing Reynolds number. One may visualize a train of rolling vortices within the boundary layer, causing a continuous exchange of mass between a zone with a very low velocity and the high velocity main flow. The extent of momentum exchange decreases as the average size of the vortices decreases.

In two-phase flow the presence of bubbles or droplets clearly has an additional effect on the size of the rolling vortices. The presence of particles within the flow increases the size (diameter) of the vortex streaks and, accordingly, produces an increased rate of dissipation of momentum from the main flow to the viscous sublayer.

In the case of liquid flow with bubbles one may expect that at least some of the bubbles form centers of rotation for a layer of surrounding liquid. Therefore, the size of the rolling vortices must depend on physical properties, which govern the size of the bubbles as well as on the flow velocity, which generates torque.

4. THE EFFECT OF VORTICES ON PHASE DISTRIBUTION

There clearly exists a field of accelerations within and around each rolling vortex close to the walls. An analysis of these accelerations is given later. The accelerations produce different inertial forces on phases with different densities. This may be called the wall-vortex effect.

In the case of bubbles in liquid flow, the acting forces are centripetal and tend to collect the bubbles on the centerlines of the vortex streaks. This accounts for the peaking of local vapor volume fraction at some small distances from the channel walls. As the population of bubbles in liquid flow increases, the average size of the rolling vortices also increases due to agglomeration of the concentrated bubbles. After a certain limit depending on channel geometry, the bubble layers on the opposite walls of a conduit may touch each other and form a core of mostly continuous vapor phase. At this point the continuity of the rotating liquid masses is disrupted.

With further increase in vapor flow a regular pattern of rolling vortices appears within the continuous vapor phase, moving close to the interface with a liquid film on the conduit wall. These vapor vortices also generate a field of centrifugal forces acting on the liquid droplets, tending to throw them either onto the liquid film or into the vapor core. At sufficiently high vapor velocities, which are expected to produce strong rotations, it should be possible to detect a zone of relatively low droplet concentration near the interface with the liquid film. This zone corresponds to the loci of the centerlines of the rolling vortices.

Such a tendency is indeed detectable according to the data reported by Cousins & Hewitt (1968). They measured the rate of droplet diffusion between the core of an annular flow and the liquid film on the wall. The experiments were carried out on a round tube of 31.75 mm I.D. The measuring technique was based on injecting a dye into the liquid film and measuring its radial distribution at various distances from the injection points by using an isokinetic sampling probe. The rate of droplet diffusion was related to the measured dye distribution. The isokinetic sampling technique was also used to measure vapor and liquid mass velocities at various radial positions. Data were collected at two different air flow rates.

The measured radial distributions of droplet mass velocities demonstrate a trend which agrees with the above mentioned prediction. Figures 4 and 5, reproduced from Cousins & Hewitt (1968), show a minimum of the local liquid mass velocities at relative radial distances of 0.42 and 0.2 from the wall. These data clearly demonstrate the influence of increased gas flow rate on the reduction of droplet concentration in the region of gas rotation centers (as hypothesised) and on a shift of this region closer to the film interface.

If, as speculated here, the rolling vortices are generated and move within the vapor phase in a zone close to the interface, they can be expected to act as a partial barrier to smaller droplets (owing to the associated centrifugal effect), thus hampering the diffusion of droplets between the liquid film and the vapor core. This explanation is in good agreement with the reported data. Figures 6 and 7 show the minima of dye and droplet diffusion coefficients in a zone near the interface with the liquid film. The interesting fact is that according to the data, the depression of the diffusion coefficients becomes more pronounced as the rate of air flow increases. Obviously, the centrifugal effect of the gas vortices increases with the flow rate of this phase. In the absence of a difference in density between the suspended particles and the main flow, the increased gas velocity increases eddy diffusivity.

Finally, the local flow pattern within the liquid film can be studied in terms of the occurrence of rolling vortices. If the film is so thin that it matches the thickness of a laminar layer sufficient to support the whole friction force, the velocity distribution in the film can be assumed to be linear and, in that case, there is no possibility for the formation of rolling vortices.

The flow pattern in a thick film may, however, be a combination of laminar flow in a very thin layer near the solid wall and a system of rolling vortices in contact with the vapor (interface). In this event some smaller bubbles may become confined to the liquid film if it is sufficiently thick, as a result of their attraction to the center lines of the vortex filmaments. Such bubbles may originate either in boiling on the wall or overlapping of the rolling waves on the interface (or

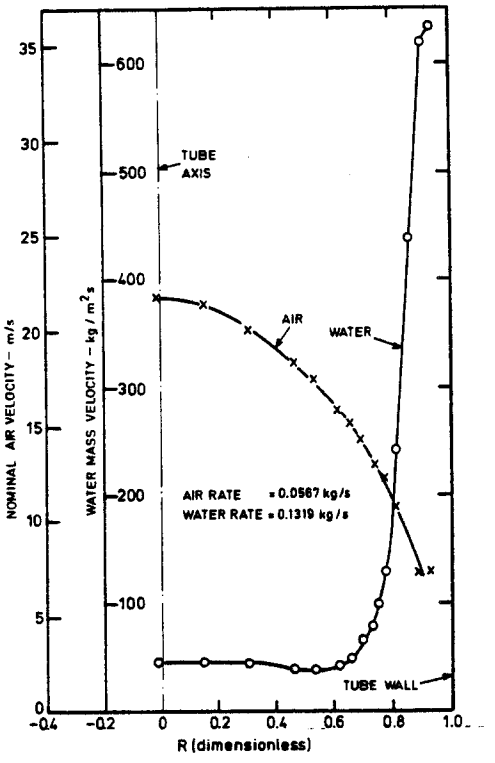

Figure 4. Mass velocity profiles obtained by the use of the isokinetic sampling probe. Data reported by Cousins & Hewitt (1968) (Source: AERE—R 5693). The liquid mass velocity shows a minimum in the vicinity of the interface.

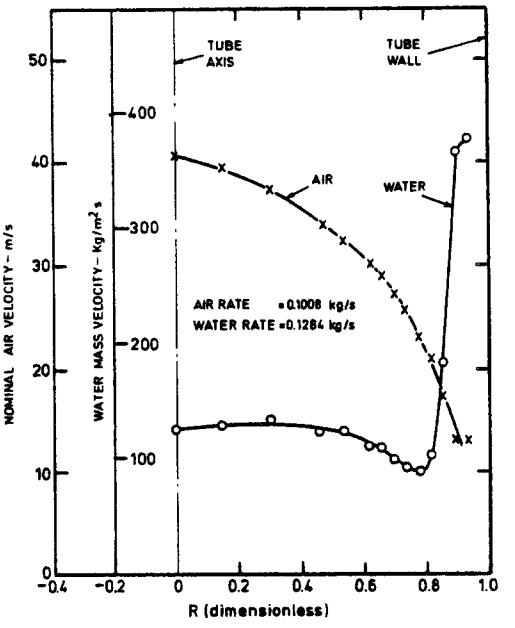

Figure 5. Mass velocity profiles obtained by the use of the isokinetic sampling probe. Data reported by Cousins & Hewitt (1968) (Source: AERE—R 5693). The liquid mass velocity shows a minimum in the vicinity of the interface.

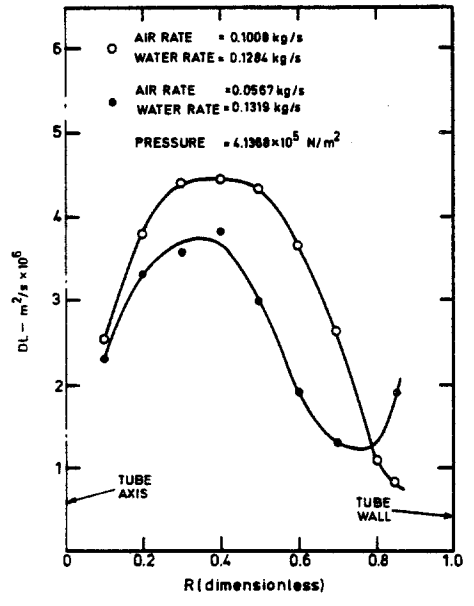

Figure 6. Dye diffusion coefficient measured across the channel. Data reported by Cousins & Hewitt (1968) (Source: AERE—R 5693). The diffusion coefficients show a minimum near the interface.

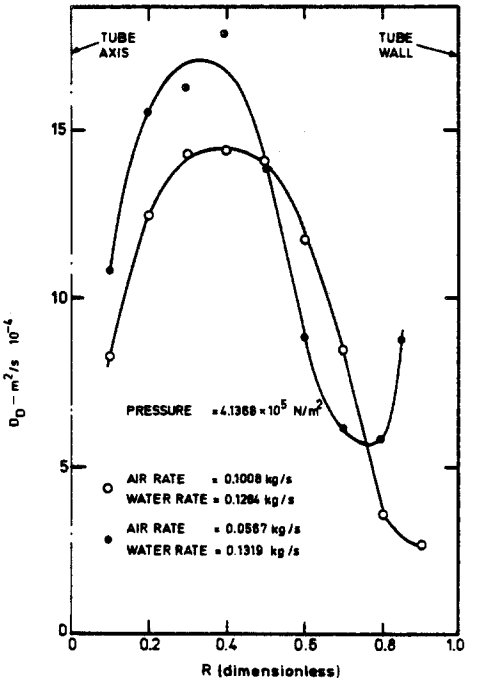

Figure 7. Diffusivity coefficient for the transport of droplets across the channel. Data reported by Cousins & Hewitt (1968) (Source: AERE—R 5693). The diffusivity coefficients are lowest near the interface.

both). The population of these bubbles is governed by the rate of their generation and the statistical chances of destruction of the rolling vortices which carry them.

5. FORMULATION AND ESTIMATION OF THE MAGNITUDE OF LOCAL ACCELERATIONS

To estimate the magnitude of forces that may develop as a result of the suggested effect, some rough calculations are presented.

5.1 *Order of magnitude of the dimensions and velocities*

No direct measurements have been made of the absolute velocity components of the fluid particles near the boundary layer nor of the loci of the rolling vortices near the walls. It thus becomes necessary to estimate these from other data that have been measured. In this connection, some measured phase-distribution profiles are used. Assuming that the position of the center lines of the rolling vortices coincide with the measured peaks of the radial void distribution, the following calculation may be performed to assess the magnitudes of acceleration and inertial forces involved in this mechanism.

As an example we consider run No. 358 of Malnes (1966) data. This is shown in figure 2. According to the data the average distance of the peaks from the wall is $\delta_r \approx 2.8$ mm.

The thickness of the viscous sublayer, δ_v is obtained from the universal velocity distribution law. According to Brodkey (1967) the non-dimensional distance from the wall at the outer edge of the viscous sublayer is about 5.5:

$$y^+ = \delta_v v_* / \nu = 5.5, \qquad [1]$$

ν is the kinematic viscosity and v_* is the shear velocity, defined by

$$v_* = \sqrt{(\tau/\rho)} = \sqrt{(\tfrac{1}{8} f \bar{U}_L^2)}.$$

Hence,

$$\delta_v = 5.5 \cdot \nu / \sqrt{(\tfrac{1}{8} f \bar{U}_L^2)}. \qquad [2]$$

Introducing the measured value of friction factor for two-phase flow, $f = 0.045$, as reported by Malnes (1966), ν for water and $\bar{U}_L = U_0/(1-\bar{\alpha})$, [2] gives $\delta_v = 0.1$ mm.

The local axial velocity at the edge of the viscous sublayer is (again according to the universal law),

$$U^+ = U_v / v_* = U_v / \sqrt{(\tfrac{1}{8} f \bar{U}_L^2)} = 5.5. \qquad [3]$$

This gives

$$U_v = 0.412 \bar{U}_L = 0.32 \text{ m/s}.$$

The average velocity of the rolling vortices along the wall is assumed to be the mean value between U_v and $\bar{U}_L$.

$$U_c = 0.5(\bar{U}_L + U_v) = 0.5(0.776 + 0.32) = 0.548 \text{ m/s}. \qquad [4]$$

The relative velocity of the vortex centers with respect to the edge of the viscous sublayer is thus

$$V_r = U_c - U_v = 0.548 - 0.32 = 0.228 \text{ m/s}. \qquad [5]$$

This corresponds to the "wheeling" velocity of the rolling vortices (or of the liquid layer around the bubbles).

5.2 *Formulation of the acceleration components*

As an easily tractable case we consider a rolling vortex on a flat wall.

The absolute velocity of a fluid particle on the periphery of this vortex has the following components (with respect to the tube wall):

$$V_a = U_c + V_r \cos \omega \qquad [6]$$

in the axial direction, and

$$V_n = -V_r \sin \omega \qquad [7]$$

normal to the wall. In these equations ω is the angular position measured from the point on the vortex circle which is tangential to the main stream as shown in figure 8. Hence

$$\frac{d\omega}{dt} = \frac{V_r}{(\delta_r - \delta_v)} \cdot \qquad [8]$$

The total acceleration vector developed by the particle motion is

$$\mathbf{a} = \frac{W^2}{R_m}\mathbf{n} + \frac{dW}{dt}\mathbf{u}, \qquad [9]$$

in which R_m is the local radius of curvature of the particle path in space and

$$W = \sqrt{(V_a^2 + V_n^2)}. \qquad [10]$$

The first term on the R.H.S. of [9] gives the local centrifugal acceleration and **n** is a unit vector in the radial direction (along R_m). The second term is the tangential acceleration and **u** is a unit vector in this direction.

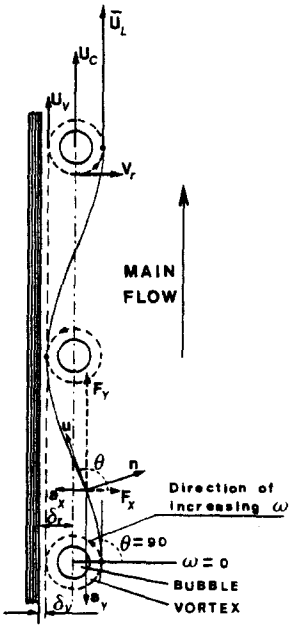

Figure 8. The idealized path of a fluid particle moving on the periphery of a wall vortex rolling in contact with the visous sublayer. F_x is the local inertial force in radial direction and F_y is the local inertial force in axial direction.

In order to evaluate R_m, **n** and **u** in [9], we consider a rectangular x–y coordinate system, the x axis normal to the channel wall and the y axis lying on the wall surface with its positive direction along the main flow. In this system the time dependent coordinates of a fluid particle, moving with velocity components V_a (along y) and V_n (along x), is

$$x = x_0 + \int_0^t V_n \, dt \quad \text{or} \quad dx = V_n \, dt, \tag{11}$$

and

$$y = y_0 + \int_0^t V_a \, dt \quad \text{or} \quad dy = V_a \, dt, \tag{12}$$

in which x_0 and y_0 are the reference coordinates at the time $t = 0$. The path of the fluid particle in this coordinate system is shown in figure 8.

Through the mathematical operations given in appendix A, it is possible to show that the total acceleration **a** may be expressed in terms of U_c, V_r and ω and that the vector **a** has components a_x normal to the wall and a_y parallel with the wall. These components are [see appendix A]

$$a_x = -V_r^2 \cos \omega / (\delta_r - \delta_v), \tag{13}$$

and

$$a_y = -V_r^2 \sin \omega / (\delta_r - \delta_v). \tag{14}$$

At each point along its path the fluid particle is subject to an inertial force proportional to its mass and the local magnitude of acceleration. The inertial force acts against the direction of acceleration.

The above given formulas are for rolling vortices along a flat wall. Similar derivations for curved surfaces include additional acceleration components due to the effect of divergence and convergence in the flow path as the particles approach or depart the wall. The combined effects rolling vortices and the local curvature of wall periphery produce stronger inertial forces acting away from a convex surface (e.g. outside surface of a tube) as compared to the inertial forces produced on concave surface (e.g. inside wall of a tube).

In the following examples the numerical values of a_x and a_y, are calculated approximately, according to the above given equations for flat wall vortices.

5.3 *Numerical examples*

We consider the numerical values of δ_r, δ_v, U_c and V_r calculated in part 5.1. This case relates to experiments with a superficial liquid velocity of $U_0 = 0.5$ m/s. The calculated values of a_x and a_y for different values of angular position ω are given in table 1. It is seen that even with this relatively low liquid velocity the local radial acceleration attains the maximum value of 19.253 m/s^2, which is almost 2 *g*. This acceleration changes sign when the fluid particle crosses the loci of the rotation center. It may be concluded that, as speculated before, the effect of the rolling vortices is generation of a field of forces that throw the heavier particles away from the rotation centers and cause a concentration of the lighter component on the loci of these centers.

Next we consider an example with liquid velocity $U_0 = 1.5$ m/s, considering the reduction in δ_r, as indicated by the data on run No. 364 in figure 2. Repeating the calculation steps according to [1]–[5] and introducing the results in [13]–[14] for different values of ω yields the axial and radial accelerations given in table 2. According to these calculations the extent of local accelerations in this case may reach some high values around 293.50 m/s^2 or about 30.0 g.

As an example of the effect of rolling vortices on liquid droplets in vapor flow, only one case of the data reported by Cousins & Hewitt (1968) will be considered.

Table 1. Axial and radial accelerations calculated for Run No-358 of Malnes data (1966)

Angle ω (degrees)	Axial acceleration (m/s^2)	Radial acceleration (m/s^2)
0.0	0.000	−19.253
15.0	−4.983	−18.597
30.0	−9.627	−16.674
45.0	−13.614	−13.614
60.0	−16.674	−9.627
75.0	−18.597	−4.983
90.0	−19.253	0.000
105.0	−18.597	4.983
120.0	−16.674	9.627
135.0	−13.614	13.614
150.0	−9.627	16.674
165.0	−4.983	18.597
180.0	0.000	19.253
195.0	4.983	18.597
210.0	9.627	16.674
225.0	13.614	13.614
240.0	16.674	9.627
255.0	18.597	4.983
270.0	19.253	0.000
285.0	18.597	−4.983
300.0	16.674	−9.627
315.0	13.614	−13.614
330.0	9.627	−16.674
345.0	4.983	−18.597
360.0	0.000	−19.253

Table 2. Axial and radial accelerations calculated for Run No-364 of Malnes data (1966)

Angle ω (degrees)	Axial acceleration (m/s^2)	Radial acceleration (m/s^2)
0.0	0.000	−293.516
15.0	−75.968	−283.515
30.0	−146.758	−254.193
45.0	−207.547	−207.547
60.0	−254.193	−146.758
75.0	−283.515	−75.968
90.0	−293.516	0.000
105.0	−283.515	75.968
120.0	−254.193	146.758
135.0	−207.547	207.547
150.0	−146.758	254.193
165.0	−75.968	283.515
180.0	0.000	293.516
195.0	75.968	283.515
210.0	146.758	254.193
225.0	207.547	207.547
240.0	254.193	146.758
255.0	283.515	75.968
270.0	293.516	0.000
285.0	283.515	−75.968
300.0	254.193	−146.758
315.0	207.547	−207.547
330.0	146.758	−254.193
345.0	75.968	−283.515
360.0	0.000	−293.516

To interpret these data in terms of the present theory several assumptions have to be made to estimate δ_r, U_c and V_r. However, the final results are not critically dependent on these assumptions.

Considering the case of data obtained with an air flow rate of 0.0567 kg/s, as shown in figure 6, it is assumed that the position of the rotation centers are at the minimum of the curve, that is, roughly at 0.25 R from the wall. The thickness of the liquid film is guessed (from the curve) to be at about 0.15 R from the wall. Considering that R = 15.875 mm, one obtains $\delta_r \cong 0.00159$ m. The laminar sublayer between the air and the interface is not considerable. Hence $\delta_v = 0$.

With the above assumptions the average air velocity is $V_A = 20.56$ m/s and the average liquid velocity in the film is $V_L = 0.6$ m/s. It is assumed that the velocity profile in the liquid film is linear and that the local velocity at the film–air interface is $2 \times V_L = 1.2$ m/s. This should be used as was U_V in the previous examples. It then follows that $U_c = 0.5\ (U_V + V_A) = 10.88$ m/s and $V_r = V_A - U_c = 9.68$ m/s.

These values are used in [13]–[14] for different ω and the results given in table 3.

It is seen that the local accelerations around a rolling vortex in the gas phase are very strong in this case. Obviously, not all of the droplets are subject to such a strong acceleration field, as the estimated vortex radius is about 1.6 mm and larger droplets are not totally dragged by the rotating air velocity. However, these calculations do support the hypothesis that, if some rolling vortices are produced in the gas flow near the interface, they are capable of acting as a partial barrier against some small droplets preventing them from being deposited on the film. This effect is bound to produce a zone of reduced droplet concentration as was discussed in previous sections and observed in experiments.

Similar calculations in the case of data with higher air flow rate give much higher values of acceleration.

In order to study the effect of some rigidity in the movement of the droplets in a gas vortex, the above calculations were repeated with reduced values of V_r, indicating some relative velocity between the air and the liquid droplets. The results of one such calculation with a velocity ratio of

Table 3. Axial and radial accelerations calculated for the low air flow tests of Cousins & Hewitt (1968) with no relative velocity

Angle ω (degrees)	Axial acceleration (m/s^2)	Radial acceleration (m/s^2)
0.0	0.0	−58932.33
15.0	−15252.81	−56924.26
30.0	−29466.17	−51036.89
45.0	−41671.45	−41671.45
60.0	−51036.89	−29466.16
75.0	−56924.26	−15252.81
90.0	−58932.33	0.00
105.0	−56924.26	15252.81
120.0	−51036.89	29466.16
135.0	−41671.45	41671.45
150.0	−29466.17	51036.89
165.0	15252.81	56924.26
180.0	0.00	58932.33
195.0	15252.81	56924.26
210.0	29466.17	51036.89
225.0	41671.45	41671.45
240.0	51036.89	29466.16
255.0	56924.26	15252.81
270.0	58932.33	0.00
285.0	56924.26	−15252.81
300.0	51036.89	−29466.16
315.0	41671.45	−41671.45
330.0	29466.17	−51036.89
345.0	15252.81	−56924.26
360.0	0.00	−58932.33

Table 4. Axial and radial accelerations calculated for the low air flow tests of Cousins & Hewitt (1968) with slip = 10

Angle ω (degrees)	Axial acceleration (m/s^2)	Radial acceleration (m/s^2)
0.0	0.00	−589.32
15.0	−152.53	−569.24
30.0	−294.66	−510.37
45.0	−416.71	−416.71
60.0	−510.37	−294.66
75.0	−569.24	−152.53
90.0	−589.32	0.00
105.0	−569.24	152.53
120.0	−510.37	294.66
135.0	−416.71	416.71
150.0	−294.66	510.37
165.0	−152.53	569.24
180.0	0.00	589.32
195.0	152.53	569.24
210.0	294.66	510.37
225.0	416.71	416.71
240.0	510.37	294.66
255.0	569.24	152.53
270.0	589.32	0.00
285.0	569.24	−152.53
300.0	510.37	−294.66
315.0	416.71	−416.71
330.0	294.66	−510.37
345.0	152.53	−569.24
360.0	0.00	−589.32

10 are given in table 4. It may be seen that even with such a high velocity ratio the local accelerations are very high compared with gravity and even in this case, the pure rotational effect produces a zone of reduced droplet concentration around the loci of the rolling vortices.

6. SOME ADDITIONAL EFFECTS OF THE ROLLING VORTICES IN TWO-PHASE FLOW

If one accepts the suggested hypothesis of (a) generation of the rolling vortices near the walls, and (b) dependence of their rotational speed on the local axial velocity in the vicinity of the channel walls, it follows that several effects in two-phase flow may be explained in terms of this mechanism. Some of these effects have already been observed in experiments. A few more may be predicted, hypothetically, as a natural consequence of this theory. Some of these effects, are now described.

6.1 *Low velocity ratio*

The average axial velocity of the layer that includes the rolling vortices is less than the mean flow velocity. According to the rough calculations performed for the above mentioned cases of Malnes (1956) data the axial velocity of these layers is expected to be 0.548 m/s in the first case and 1.274 in the second. Both values are less than average liquid velocities. Hence, as far as these layers are concerned, the gas phase has an upward velocity less than that of the liquid phase. However, the average gas velocity over the channel area as a whole is higher, due partly to the rising velocity of the bubbles outside of the boundary layer and partly to the extra buoyancy of the boundary layer. One consequence of this effect is that velocity ratios less than unity are to be expected at low void fraction and high liquid velocity. Figure 9, which is a further extract from Malnes (1966) data, supports this conclusion.

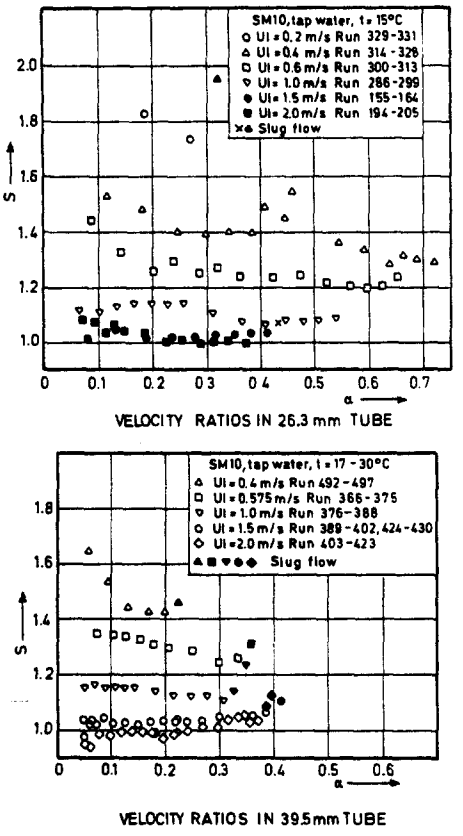

Figure 9. Demonstration of the effects of liquid velocity, average void and other parameters on relative velocity in vertical upward flow. Data reported by Malnes (1966) (Source: KR–110).

6.2 *Reduced mixing of the vapor phase between subchannels*

Repeated experiments performed on mixing between subchannels in two-phase flow have consistently posed a dilemma; the vapor phase mixing decreases with increasing liquid velocity, while the liquid phase mixing improves with velocity. Experimental evidence of these observations is reported by Rowe & Angle (1969), van der Rose (1970) and Rudzinski *et al.* (1973).

Before any attempt is made to explain the effect of rolling vortices on vapor mixing it should be pointed out that the relatively low rate of vapor mixing is observed only in the bubbly flow regime. The mixing rate improves considerably when the flow regime is changed to slug flow, and particularly at the transition to annular flow. Another point that must be observed is the distinction between vapor mixing and diversion cross-flow, namely that the latter increases with the onset of steam generation in one subchannel.

It has already been stated that when the liquid phase is continuous, the rolling vortices near the walls can be expected to arrest many of the bubbles. The intensity of vortex generation and the rotational speed should be strongest at the positions of highest velocity gradient normal to the walls. The cross-sectional view of the common types of subchannel and the typical patterns of velocity distribution in those subchannels are shown in figure 10. Consideration of this diagram indicates that, except in the case of the corner subchannel with an annular shape, the strongest velocity gradients occur at positions remote from the gaps. It then follows that the vapor bubbles are rather isolated from the path of flow mixing, and hence vapor mixing is poor in a bubbly flow regime., with the exception of such exchanges as occur between a corner subchannel of annular shape and a side subchannel. According to this explanation the effect of vapor mixing in the latter instance should be rather one sided (owing to a relatively higher contribution by the vapor in the corner subchannel). Unfortunately, this particular test geometry has not been studied in any of the reported mixing experiments.

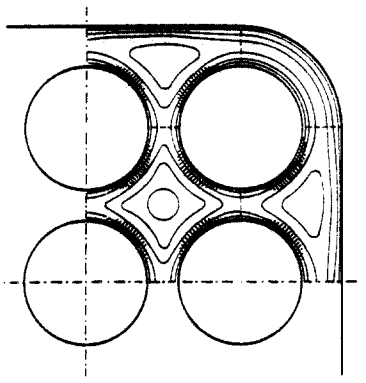

Figure 10. A sketch of the common subchannel types and the regions of bubble concentration in low quality boiling. The shaded areas indicate the zones of higher velocity gradients and more intensive vortex generation.

With this argument as a basis it is evident that a relevant method of mixing calculation in two-phase flow must include, in addition to the effect of flow regime, a representation of the subchannel geometry and the factors which influence the radial velocity gradients. The ordinary concept of equivalent hydraulic diameter is not an adequate description of the geometry.

6.3 *Dry-out position in rod bundles*

The arguments stated above should be equally valid in analyzing burn-out or dry-out conditions on the heated rods around subchannels. Referring to the effect of vapor vortices in reducing droplet diffusion from the main flow to the walls, it should be expected that those parts of a rod that face the center of a subchannel, and produce the highest velocity gradient, should be subject to dryout before the other parts of the same rod. This is to say that with a constant heat flux around a rod the dry-out should always begin at some spot facing the center of a subchannel. The gap regions are less deprived of droplet deposition and hence should show dry-out at some later stages. No published data on exact position of dry-out in subchannels have been found to examine this hypothesis.

6.4 *Suppression of surface tension in flashing bubbles*

If it is assumed that the angular velocity is uniform within each rolling vortex, that is to say, from its outer radius R to the bubble radius r_b, then the relationship between the static pressures, p_b in the bubble and p_L in the bulk liquid flow is

$$p_b = p_L + 2\sigma/r_b - \rho_L(R - r_b)V_r^2/R \qquad [15]$$

where σ is the surface tension, ρ_L is the liquid density, and V_r is the "wheeling" speed of the rolling vortex as defined in part 5.

The third term on the R.H.S. of the above equation shows the effect of wall vortex on reducing bubble pressure. This is equivalent to a reduction in the amount of liquid superheat required for the continuation of flashing. It should be noted that the effect of this term is gained separately from the results of depressurization due to the linear acceleration of the liquid. Based on this argument, the rate of flashing of a flowing depressurized liquid should depend to some extent, on the flow velocity and its gradient near the walls.

6.5 *Secondary flows*

Secondary flows in non-circular geometries have been observed and reported by several investigators. Some classical examples are given by Schlichting (1960) and detailed studies of local secondary flows in various parts of some different subchannels are reported by Rowe

(1973). These flow patterns, which have been studied in single-phase flow may be suitably interpreted in terms of the effect of rolling vortices along the walls.

According to the formulas given in section 5.2 and in appendix A the magnitude of the local inertial force in radial direction depends on the vortex rotation intensity. The rotation intensity is expected to be higher near the walls that have higher normal velocity gradients. This means that, in such positions, the fluid particles are thrown away from the wall more strongly than in the other parts of the channel, where the velocity gradients normal to the wall are relatively weaker. This generates a flow circulation on the planes perpendicular to the main flow. This explanation matches the observed flow behaviour.

7. CONCLUSION

The hypothesis of generation of rolling vortices near the walls offers acceptable explanations for a number of peculiarities in flow systems, especially in two-phase flow.

The intensity and size of the rolling wall vortices depends on the local velocity gradients. Hence a proper formulation of mathematical models for calculation of the above mentioned behaviour must be based on those physical factors which influence the local velocity gradients normal to the wall.

REFERENCES

BRODKEY, R. S. 1967 *The Phenomena of Fluid Motions.* Addison–Wesley, Reading, Mass.

COUSINS, L. B. & HEWITT, G. F. 1968 Liquid phase mass transfer in annular two-phase flow: radial liquid mixing. AERE-R 5693.

DIX, G. E. 1971 Vapor void fractions for forced convection with subcooled boiling at low flow rates. NEDO-10491.

EICHHORN, R. & SMALL, S. 1964 Experiments on lift and drag of spheres suspended in a Poiseuille flow. *J. Fluid Mech.* **20**, 513–527.

JEFFREY, R. C. & PEARSON, J. R. A. 1965 Particle motion in laminar vertical tube flow. *J. Fluid Mech.* **22**, 721–735.

KLINE, S. J., REYNOLDS, W. C., SCHRAUB, F. A. & RUNSTADLER, P. W. 1967 The structure of turbulent boundary layers. *J. Fluid Mech.* **30**, 741–773.

KROEGER, P. G. & ZUBER, N. 1966 A program of two-phase flow investigation: thirteenth quarterly report. GEAP-5203.

LIGHTHILL, M. J. 1963 *Laminar boundary Layers*, pp. 96–102 (Rosenhead, L., Ed.). Clarendon Press, Oxford.

MALNES, D. 1966 Slip ratios and friction factors in the bubble flow regime in vertical tubes. KR-110.

OLIVER, D. R. 1962 Influence of particle rotation on radial migration in the Poiseuille flow of suspensions. *Nature, Lond.* **194**, 1269–1271.

ROWE, D. S. 1973 Measurement of turbulent velocity, intensity and scale in rod bundle flow channels. BNWL-1736.

ROWE, D. S. & ANGLE, C. W. 1969 Cross-flow mixing between parallel flow channels during boiling, Part III: Effect of spacers on mixing between two channels. BNWL-371.

RUDZINSKI, K. F., SINGH, K. & ST. PIERRE, C. G. 1972 Turbulent mixing for air–water flows in simulated rod bundle geometries. *Can. J. Chem. Engng* **50**, 297–299.

SCHLICHTING, H. 1960 *Boundary Layer Theory.* McGraw–Hill, New York.

SEGRÉ, G. & SILBERBERG, A. 1962 Behaviour of macroscopic rigid spheres in Poiseuille flow. Parts 1 and 2. *J. Fluid Mech.* **14**, 115–135 and 130–157.

SHIRALKAR, B. S. 1970 Local void fraction measurements in freon-114 with a hot-wire anemometer. General Electric Co. NEDE-13158.

SHIRES, L. & RILEY, P. J. 1966 The measurement of radial voidage distribution in two-phase flow by isokinetic sampling. AEEW-M650.

STAUB, F. W. & WALMET, G. E. 1969 Heat transfer and hydraulics: the effects of subcooled voids. NY0-3679-8 EURAEC-2120.

STAUB, F. W. & ZUBER, N. 1964 A program of two-phase flow investigation: Fifth quarterly report. GEAP-4631.

SWANSON, W. M. 1961 The Magnus effect: a summary of the investigations to date. *J. Bas. Engng* **83**, 461–470.

VAN DER ROS, T. 1970 On two-phase flow exchange between interacting hydraulic channels. WW015-R160.

APPENDIX A

Derivation of Acceleration Equations

From analytic geometry it is known that, for any two-dimensional curve like $y = f(x)$, the local radius of curvature R_m may be obtained from the following equation,

$$\frac{1}{R_m} = \frac{y''}{(1+y'^2)^{3/2}}\ , \qquad [A\text{-}1]$$

in which $y' = dy/dx$ and $y'' = dy'/dx$.

From [11] and [12] in combination with [6] and [7] one obtains

$$y' = V_a/V_n = -(U_c + V_r \cos\omega)/V_r \sin\omega. \qquad [A\text{-}2]$$

This gives

$$(1+y'^2)^{3/2} = W^3/(V_r^3 \sin^3\omega), \qquad [A\text{-}3]$$

where W is defined by [10].

$$y'' = \left(\frac{dy'}{d\omega}\right)\left(\frac{d\omega}{dt}\right)\left(\frac{dt}{dx}\right) = -\frac{V_r + U_c\cos\omega}{V_r^2 \sin^3\omega}\left(\frac{d\omega}{dt}\right) \qquad [A\text{-}4]$$

in which $dt/dx = -1/\sin\omega$ is obtained by eliminating V_n between [7] and the differential form of [11].

Introducing [A-4] and [A-3] into [A-1] one obtains

$$\frac{1}{R_m} = -\frac{V_r}{W^3}(V_r + U_c\cos\omega)\frac{d\omega}{dt}\ , \qquad [A\text{-}5]$$

Hence the centrifugal acceleration term in [9] will be obtained by combining [A-5], [10] and [8]

$$\frac{W^2}{R_m}\mathbf{n} = -\frac{V_r^2}{(\delta_r - \delta_v)W}(V_r + U_c\cos\omega)\mathbf{n}. \qquad [A\text{-}6]$$

The unit normal vector $\mathbf{n}$ may be defined in terms of two orthogonal unit vectors $\mathbf{i}$ along x and $\mathbf{j}$ along y axes, and

$$\mathbf{n} = \mathbf{i}\sin\theta - \mathbf{j}\cos\theta. \qquad [A\text{-}7]$$

Here θ is the angle between a unit vector tangential to the path of the particle (following the curve of $y = f(x)$) and the positive direction of the x axis as illustrated in figure 8. From the

differential increment of the path of the fluid particle, viz. $ds = W\,dt$, in combination with [11] and [12], one obtains

$$\cos\theta = dx/ds = V_n/W, \qquad [A\text{-}8]$$

and

$$\sin\theta = dy/ds = V_a/W. \qquad [A\text{-}9]$$

The unit vectors **i** and **j** and the angle θ are employed to define the unit tangent vector **u**,

$$\mathbf{u} = \mathbf{i}\cos\theta + \mathbf{j}\sin\theta. \qquad [A\text{-}10]$$

Finally, the tangential acceleration component in [9] is

$$\frac{dW}{dt}\boldsymbol{u} = \left(\frac{dW}{d\omega}\right)\frac{d\omega}{dt}\mathbf{u} = -\frac{V_r^2 U_c \sin\omega}{(\delta_r - \delta_v)W}\mathbf{u}. \qquad [A\text{-}11]$$

The aforementioned acceleration vectors change in magnitude and direction as the fluid particle moves with a rolling vortex and completes one rotation.

One may consider the resultants of the projections of the acceleration components of **a** in the radial and axial directions. The total radial acceleration is $a_x = \mathbf{a}\cdot\mathbf{i}$ and the total axial acceleration $a_y = \mathbf{a}\cdot\mathbf{j}$. In calculating these products we observe that, by definition, $\mathbf{i}\cdot\mathbf{j} = \mathbf{j}\cdot\mathbf{i} = 0$ and $\mathbf{i}\cdot\mathbf{i} = \mathbf{j}\cdot\mathbf{j} = 1$. The result is

$$a_x = \mathbf{a}\cdot\mathbf{i} = -V_r^2\cos\omega/(\delta_r - \delta_v), \qquad [A\text{-}12]$$

and

$$a_y = \mathbf{a}\cdot\mathbf{j} = -V_r^2\sin\omega/(\delta_r - \delta_v). \qquad [A\text{-}13]$$

in which

$$\Omega = V_r^2/[(\delta_r - \delta_v)W^2]. \qquad [A\text{-}14]$$

APPENDIX B

The Magnus Effect and How it Differs from the Wall-Vortex Effect

In the literature on suspension flows there are many reports devoted to theoretical and experimental studies of the behaviour of solid particles in a flow through a tube. Among the works referred to are those of Segré & Silberberg (1962), Eichhorn & Small (1964), and Jeffrey & Pearson (1965). These studies are almost entirely limited to the behaviour of particles in laminar flow. It has been generally observed that, in laminar flow, dense particles falling slowly through a rising body of fluid migrate to the tube axis; buoyant particles in the same flow migrate to the tube wall. Conversely, dense particles falling through a descending fluid migrate to the tube walls and buoyant particles to the tube axis. Oliver (1962) observed that the radial movement of suspended spheres in a laminar flow was dependent upon their rotational spin and explained this phenomenon in terms of the Magnus effect.

The Magnus effect is well described by Swanson (1961). In the introduction to his article Swanson describes the Magnus effect in the following terms; "A spinning missile or body travelling through the air, in such a way that the body axis of rotation is at an angle with the flight

path, will experience a Magnus force component in a direction perpendicular to the plane in which the flight path and rotational axis lie".

Clearly, the relative axial velocity of a buoyant or dense particle, within the field of velocity gradient of a laminar flow inside a tube, may generate some rotation. This rotation can, in turn, be expected to develop a Magnus force which will impart a radial motion to the particle until the force is balanced by some other effect.

It should be observed that the Magnus effect is a result of the interaction of the spinning motion of a moving body with its translational motion in a medium. This is an entirely different effect from that produced by the influence of a centripetal or centrifugal force on a particle within the rotational field of a vortex. In some cases, however, the motion of suspended particles may be the result of an addition of both of these effects.